

Numerical electrokinetics

R. Schmitz¹ and B. Dünweg^{1,2}

¹ Max Planck Institute for Polymer Research, Ackermannweg 10, 55128 Mainz, Germany

² Department of Chemical Engineering, Monash University, Clayton, Victoria 3800, Australia

Abstract.

A new lattice method is presented in order to efficiently solve the electrokinetic equations, which describe the structure and dynamics of the charge cloud and the flow field surrounding a single charged colloidal sphere, or a fixed array of such objects. We focus on calculating the electrophoretic mobility in the limit of small driving field, and systematically linearise the equations with respect to the latter. This gives rise to several subproblems, each of which is solved by a specialised numerical algorithm. For the total problem we combine these solvers in an iterative procedure. Applying this method, we study the effect of the screening mechanism (salt screening vs. counterion screening) on the electrophoretic mobility, and find a weak non-trivial dependence, as expected from scaling theory. Furthermore, we find that the orientation of the charge cloud (i. e. its dipole moment) depends on the value of the colloid charge, as a result of a competition between electrostatic and hydrodynamic effects.

PACS numbers: 47.11.-j, 47.57.jd, 47.57.E-, 47.57.J-, 47.57.-s, 82.45.-h, 82.70.Dd, 82.70.-y, 05.60.Cd

1. Introduction

The interplay between electrostatic and hydrodynamic interactions is of high importance for the understanding of a wide range of biological, chemical and physical systems, since in almost all situations where a solid is brought in contact with a liquid, a difference in the electric potential occurs due to association or dissociation of charges or the orientation of molecules at the surface.

Charged solid colloidal spheres in suspension in an aqueous solution containing counterions and salt ions will be surrounded by a cloud of oppositely charged ions. This cloud, typically called the electric double layer, is responsible for screening the electrostatic potential. If an external electric field is acting on the system, the charged spheres start to migrate in the direction of the oppositely charged electrode and the surrounding cloud will be deformed and becomes anisotropic due to the electric field and also to the friction between the ions and the fluid. This phenomenon is called electrophoresis and the corresponding transport coefficient is the electrophoretic mobility μ , determined by the balance of electric driving and hydrodynamic frictional force acting on the sphere. It is defined as the proportionality constant between the constant velocity \mathbf{u} of the particle and the external driving field \mathbf{E}_{ext} in the linear regime, i. e. for small driving fields,

$$\mathbf{u} = \mu \mathbf{E}_{ext}. \quad (1)$$

Efforts have been made to study electrophoresis by experimental methods [1, 2, 3, 4, 5] as well as by analytical and numerical calculations over the decades [6, 7, 8, 9, 10, 11, 12, 13, 14, 15, 16, 17, 18, 19, 20, 21, 22, 23, 24]. Due to the complicated many-body nature of the problem a comprehensive quantitative theoretical understanding is still lacking.

An important milestone was the theoretical investigation by O’Brien and White [13], later known as “standard electrokinetic model”. Starting from the dynamic Mean-Field equations that describe the interplay between the convection-diffusion dynamics of the ion clouds, the solvent flow field, and the electrostatic forces in the system, they studied a single charged colloidal sphere in infinite space, subject to an infinitesimally weak homogeneous external electric field, with respect to which the equations are linearised. This problem exhibits full spherical symmetry, and hence its numerical treatment reduces to the solution of a one-dimensional ordinary differential equation, which finally allows the calculation of μ .

This approach has a fairly broad but not unlimited range of applicability, whose conditions may be summarised as follows: Firstly, the Mean-Field theory as such must be justified, and this implies weak ion-ion correlations, which is typically the case for single-valence ions at room temperature. Furthermore, treating the problem within the framework of a single-colloid theory requires that the ionic clouds essentially do not overlap, and all non-trivial values of charge density, electrostatic potential, and flow velocity are confined to the double layer, as a result of electrostatic and hydrodynamic screening. This means that the salt concentration has to be fairly large, and the

electrostatic screening is dominated by the salt contribution: Note that for a single sphere in infinite space the counterions have all entropically “evaporated”, and hence must be ignored in the theory.

It is exactly this latter condition that is violated in recent experiments on colloidal electrophoresis [1, 22], which have deliberately focused on the limit of low salt. In Ref. [22] it was shown that some (certainly not all) experimental observations in that regime can be explained by assuming that the effects of finite colloid volume fraction (and corresponding finite counterion concentration) can be modeled by simply studying a single colloidal particle in a finite simulation box with periodic boundary conditions, which automatically gives rise to a finite colloid volume fraction and the correct corresponding counterion concentration. This investigation was done by studying a system of charges by Molecular Dynamics, while the solvent hydrodynamics was taken into account by a Lattice Boltzmann background. However, the computational effort of such studies turned out to be large, such that it was neither possible to obtain highly accurate results, nor to vary parameters systematically over a broad range.

For these reasons, we develop a new approach in the present paper: On the one hand, we wish to study precisely the same physical situation as in Ref. [22], i. e. a single colloidal particle in a finite box with a finite counterion concentration, possibly with added salt, while on the other hand taking full advantage of the O’Brien and White approach, which means that we study the Mean-Field equations, combined with linearisation with respect to the driving field. In summary, our work is nothing more and nothing less than the finite-volume generalisation of Ref. [13], whose results are directly recovered in the special limit of large salt concentration, where the double layer is significantly smaller than the box. Our method is based upon a full three-dimensional calculation, where the partial differential equations are discretised on a lattice. Since these equations are mathematically fairly different, we develop specialised solvers for each equation. The colloidal particle acts essentially as a boundary condition, and hence it is clear that the method can be easily generalised to a fixed array of particles or any other object that is periodically repeated in space — strictly spoken, we are studying a colloidal crystal, as a result of the periodic boundary conditions of the box. Within this setup one may vary several important parameters like volume fraction and averaged ion concentrations, and study the behaviour of μ fairly accurately.

Returning to the issue of the limitations of the present approach, we notice that the present model differs from the Molecular Dynamics / Lattice Boltzmann (MD/LB) model not only with respect to its computational cost, but also in terms of the modeling of the finite size of the ions. The present model clearly assumes point ions and neglects any ion-ion correlations, which, however, due to packing effects, are important if the colloid size is not very large compared to the ion size [15, 16]. On the other hand, these correlations are fully present in the MD/LB model. However, it should be noted that the MD/LB model is, for computational reasons, very limited in terms of the ratio of colloid size to ion size, which cannot have values much in excess of 10. Therefore, the MD/LB model will probably, in comparison to experiment, overestimate the effects of packing

and ion correlations, except for quite small colloids. We therefore study here the other extreme, which should be reasonable for large colloids. While there are attempts to include the finite size of ions into more generalised Mean Field theories, both for statics [15, 16, 25] and dynamics [15, 16], it is not immediately obvious how to incorporate these formalisms into a three-dimensional code that is strictly confined to a finite box with a well-defined and conserved number of ions. Furthermore, the present model should be viewed as just a first step to the development of a more general simulation program that is able to study multi-colloid systems. At finite volume fraction, colloid-colloid correlations are quite important, and they are of course not taken into account by our “cell” or “colloidal crystal” model. For the statics, the importance of such correlations has been pointed out, e. g., in Refs. [26, 27]; in the dynamic case one expects a probably even stronger effect, since here not only the electrostatic interactions are insufficiently screened, but the hydrodynamic interactions as well. A multi-colloid simulation model with explicit ions is however very likely to be computationally too expensive, except for very moderate scale separations between macro- and micro-ions, both with respect to length and with respect to charge. The present work is intended as a first step in an attempt to overcome at least the former of these limitations, by assuming full scale separation between length scales at the outset. Of course, numerically this scale separation is anything but perfect, due to limited grid resolution; however, discretised field theories seem to be more amenable to extrapolation procedures than particle models.

In Sec. 2 the theoretical model is introduced, including the Mean-Field approach and the linearisation of the equations. Furthermore, the equations are reformulated in dimensionless units. The computational method is briefly discussed in Sec. 3, where we describe the iterative combination of the specialised solvers and discuss the particular choices for the numerical methods. In Sec. 4 some interesting results from this method are presented: The dependence of the electrophoretic mobility on the details of the screening mechanism is analysed, and the reversal of the field-induced dipole moment of the ion cloud surrounding a weakly charged colloid is elucidated. Section 5 concludes with a brief summary.

2. Theory

2.1. Electrokinetic equations

Electrophoresis is a result of the balance between electrostatics and hydrodynamics. Within a Mean-Field picture the system is described in terms of ion concentration fields c_i , electrostatic potential ψ and the flow velocity field \mathbf{v} . Cross-correlations between salt ions as well as thermal fluctuations are neglected.

The Poisson equation couples the concentration fields to the electrostatic potential,

$$-\nabla^2\psi = \frac{1}{\varepsilon}e \sum_i z_i c_i. \quad (2)$$

Here, ε is the dielectric constant, e denotes the elementary charge and z_i is the valence of the ionic species, where the subscript i indicates the different ionic species in the system. Counterions, which assure the charge neutrality of the system, are denoted by the index $i = 0$. The charged colloids are taken into account via boundary conditions.

The dynamics of the concentration field c_i is described by a continuity equation, where the total current density is a combination of a diffusive term, a convective current and the current resulting from the electric force. One thus obtains a convection–diffusion equation, known as Nernst–Planck equation,

$$\partial_t c_i = \nabla \cdot \left(D_i \nabla c_i + \frac{D_i}{k_B T} e z_i (\nabla \psi) c_i - \mathbf{v} c_i \right). \quad (3)$$

Here, D_i is the diffusion constant of the ionic species i and $k_B T$ denotes the thermal energy. The ion mobility is given by $D_i/(k_B T)$ due to the Einstein relation.

Electric forces and viscous forces are balanced in the Stokes equation which describes zero Reynolds number incompressible hydrodynamics,

$$\nabla \cdot \mathbf{v} = 0, \quad (4)$$

$$\rho \partial_t \mathbf{v} = -\nabla p + \eta \nabla^2 \mathbf{v} - e (\nabla \psi) \sum_i z_i c_i, \quad (5)$$

where ρ is the mass density of the fluid, p its pressure field and η the fluid viscosity.

In the stationary state, the system of equations is thus summarised as [28]

$$0 = \nabla^2 \psi + \frac{1}{\varepsilon} e \sum_i z_i c_i, \quad (6)$$

$$0 = \nabla \cdot \left(D_i \nabla c_i + \frac{D_i}{k_B T} e z_i (\nabla \psi) c_i - \mathbf{v} c_i \right), \quad (7)$$

$$0 = -\nabla p + \eta \nabla^2 \mathbf{v} - e (\nabla \psi) \sum_i z_i c_i, \quad (8)$$

$$0 = \nabla \cdot \mathbf{v}. \quad (9)$$

Notice that the stationary formulation is not manifestly Galilei invariant, but rather selects one particular frame of reference (the rest frame of the colloidal particle) in which it is valid. If a colloidal sphere would move relative to the chosen inertial frame, the local ionic concentration would change with time, and hence a stationary solution would not exist. It is this restriction which either confines the method to single–colloid studies, or forces us to impose a somewhat unphysical “rigid–body” constraint between the set of colloidal particles. The mobility however is measured in the system’s center–of–mass reference frame. In other words, the center–of–mass velocity of the system must be taken as the velocity that determines μ . As a matter of fact, it turned out that it is most convenient to solve the Nernst–Planck equation in the colloid rest frame, while the Stokes equation is best solved in the rest frame of the center of mass. Therefore, one always needs a trivial Galilei transform when switching from one equation to the other.

2.2. Dimensionless formulation

An important length scale in the theory of charged systems is the Bjerrum length, which results from the balance between electrostatic and thermal energy:

$$l_B = \frac{e^2}{4\pi\epsilon k_B T}. \quad (10)$$

The Stokes mobility of a sphere of radius l_B and elementary charge e provides a natural unit for the electrophoretic mobility:

$$\mu_0 = \frac{e}{6\pi\eta l_B}, \quad (11)$$

and the dimensionless reduced electrophoretic mobility is defined as

$$\mu_{red} = \frac{\mu}{\mu_0}. \quad (12)$$

The natural energy scale is the thermal energy $k_B T$, and together with the elementary charge e this yields a dimensionless electrostatic potential

$$\tilde{\psi} = \psi \frac{e}{k_B T}. \quad (13)$$

Introducing a second length scale κ^{-1} (see below), such that the gradient is rescaled via

$$\tilde{\nabla} = \frac{1}{\kappa} \nabla, \quad (14)$$

the electrokinetic equations are nondimensionalised as

$$0 = \tilde{\nabla}^2 \tilde{\psi} + \sum_i z_i \tilde{c}_i, \quad (15)$$

$$0 = \tilde{\nabla} \cdot \left(\tilde{D}_i \tilde{\nabla} \tilde{c}_i + \tilde{D}_i z_i (\tilde{\nabla} \tilde{\psi}) \tilde{c}_i - \tilde{\mathbf{v}} \tilde{c}_i \right), \quad (16)$$

$$0 = -\tilde{\nabla} \tilde{p} + \frac{2}{3} \tilde{\nabla}^2 \tilde{\mathbf{v}} - (\tilde{\nabla} \tilde{\psi}) \sum_i z_i \tilde{c}_i, \quad (17)$$

$$0 = \tilde{\nabla} \cdot \tilde{\mathbf{v}}, \quad (18)$$

where the dimensionless parameters and variables are summarised in Tab. 1.

Note that the transformation from physical to reduced units, as outlined in Tab. 1, is valid for any arbitrary choice of the length scale κ^{-1} . However, a physically motivated choice results from the finite-volume version of linearised Poisson-Boltzmann theory (Debye-Hückel theory). We therefore choose κ to be the Debye screening parameter,

$$\kappa^2 = 4\pi l_B \sum_i z_i^2 \frac{N_i}{V}, \quad (19)$$

where all ionic species (including the counterions) contribute, V is the volume of the system (actually the volume that is available to the ions, i. e. box volume minus colloid volume), and N_i the number of ions of species i . For simplicity the tilde will from now on be omitted, with the understanding that all parameters are given in reduced units.

parameter	physical units	dimensionless formulation
Bjerrum length	$l_B = \frac{e^2}{4\pi\epsilon k_B T}$	
screening parameter	$\kappa^2 = 4\pi l_B \sum_i z_i^2 \frac{N_i}{V}$	
electrophoretic mobility	μ	$\mu_{red} = \frac{6\pi\eta l_B}{e} \mu$
spatial position	\mathbf{r}	$\tilde{\mathbf{r}} = \kappa \mathbf{r}$
spatial derivative	∇	$\tilde{\nabla} = \frac{1}{\kappa} \nabla$
electrostatic potential	ψ	$\tilde{\psi} = \frac{e}{k_B T} \psi$
electric field	\mathbf{E}	$\tilde{\mathbf{E}} = \frac{e}{\kappa k_B T} \mathbf{E}$
ion concentration	c_i	$\tilde{c}_i = \frac{4\pi l_B}{\kappa^2} c_i$
colloid charge	Ze	$\tilde{Z} = 4\pi l_B \kappa Z$
number of ions	N_i	$\tilde{N}_i = 4\pi l_B \kappa N_i$
flow velocity	\mathbf{v}	$\tilde{\mathbf{v}} = \frac{6\pi l_B \eta}{\kappa k_B T} \mathbf{v}$
pressure	p	$\tilde{p} = \frac{4\pi l_B}{\kappa^2 k_B T} p$
diffusion constant	D_i	$\tilde{D}_i = \frac{6\pi l_B \eta}{k_B T} D_i$

Table 1. Summary of all parameters in physical units and their reduced counterparts.

2.3. Linearisation

The high nonlinearity of the Mean-Field equations causes two problems. Firstly, it is difficult and computationally expensive to solve a coupled system of nonlinear differential equations. Furthermore, the electrophoretic mobility is well-defined (i. e. independent of the driving field) only in the linear regime. Consequently, if a fully nonlinear solution of the equations is obtained, an extrapolation to zero driving field is required. The second problem can be avoided completely, and the first one at least reduced, by a linearisation of the equations in terms of the driving field [13, 28]. This can be done by a formal expansion with respect to a small parameter ϵ , corresponding to the strength of the external field. All fields in the system have a regular expansion

in ϵ , and hence may be written as

$$c_i = c_i^{(0)} + \epsilon c_i^{(1)} + \mathcal{O}(\epsilon^2), \quad (20)$$

$$\psi = \psi^{(0)} + \epsilon \psi^{(1)} + \mathcal{O}(\epsilon^2), \quad (21)$$

$$\mathbf{v} = \epsilon \mathbf{v}^{(1)} + \mathcal{O}(\epsilon^2), \quad (22)$$

$$p = p^{(0)} + \epsilon p^{(1)} + \mathcal{O}(\epsilon^2); \quad (23)$$

note that for $\epsilon = 0$, i. e. in the absence of external driving, the system is at rest, such that the zeroth-order velocity vanishes. We now insert the expansion into the electrokinetic equations; noticing that for $\epsilon = 0$ all ionic currents must vanish, one obtains

- in zeroth order perturbation theory:

$$0 = \nabla^2 \psi^{(0)} + \sum_i z_i c_i^{(0)}, \quad (24)$$

$$0 = \nabla \cdot \left(z_i \psi^{(0)} + \ln c_i^{(0)} \right), \quad (25)$$

$$0 = -\nabla p^{(0)} - (\nabla \psi^{(0)}) \sum_i z_i c_i^{(0)}. \quad (26)$$

- and in first order:

$$0 = \nabla \cdot \left\{ D_i \nabla c_i^{(1)} + D_i z_i (\nabla \psi^{(1)}) c_i^{(0)} + D_i z_i (\nabla \psi^{(0)}) c_i^{(1)} - \mathbf{v}^{(1)} c_i^{(0)} \right\}, \quad (27)$$

$$0 = -\nabla p^{(1)} + \frac{2}{3} \nabla^2 \mathbf{v}^{(1)} - (\nabla \psi^{(1)}) \sum_i z_i c_i^{(0)} - (\nabla \psi^{(0)}) \sum_i z_i c_i^{(1)}, \quad (28)$$

$$0 = \nabla \cdot \mathbf{v}^{(1)}, \quad (29)$$

$$0 = \nabla^2 \psi^{(1)} + \sum_i z_i c_i^{(1)}. \quad (30)$$

The zeroth order only contains the electrostatic potential of the unperturbed ion clouds; hence this order is identical to standard nonlinear Poisson–Boltzmann theory. Equation 26 is just an equation to determine the zeroth-order pressure, which is of no interest to us; it can therefore be simply ignored. The first order consists of a coupled set of *linear* equations; hence the only nonlinearity that remains is the equilibrium Poisson–Boltzmann problem, which is simpler than studying the original full set of nonlinear dynamic equations.

In the first-order equations, the external field is taken into account by decomposing the potential $\psi^{(1)}$ into a periodic part and one part corresponding to the constant electric field

$$\psi^{(1)} = \psi'^{(1)} + \psi''^{(1)}, \quad (31)$$

such that

$$\nabla^2 \psi'^{(1)} = - \sum_i z_i c_i^{(1)}, \quad (32)$$

$$\nabla^2 \psi''^{(1)} = 0, \quad (33)$$

$$\nabla \psi''^{(1)} = - \mathbf{E}_{ext}. \quad (34)$$

Hence one may write the first-order equations more explicitly as

$$0 = \nabla \cdot \left\{ D_i \nabla c_i^{(1)} + D_i z_i (\nabla \psi'^{(1)}) c_i^{(0)} - D_i z_i \mathbf{E}_{ext} c_i^{(0)} + D_i z_i (\nabla \psi^{(0)}) c_i^{(1)} - \mathbf{v}^{(1)} c_i^{(0)} \right\}, \quad (35)$$

$$0 = -\nabla p^{(1)} + \frac{2}{3} \nabla^2 \mathbf{v}^{(1)} - (\nabla \psi'^{(1)}) \sum_i z_i c_i^{(0)} + \mathbf{E}_{ext} \sum_i z_i c_i^{(0)} - (\nabla \psi^{(0)}) \sum_i z_i c_i^{(1)}, \quad (36)$$

$$0 = \nabla \cdot \mathbf{v}^{(1)}, \quad (37)$$

$$0 = \nabla^2 \psi'^{(1)} + \sum_i z_i c_i^{(1)}. \quad (38)$$

It should be noted that, as a result of the perturbation expansion, the first-order convection–diffusion equation now contains sources and sinks (the terms proportional to $c_i^{(0)}$). However, since these terms all have the form of a divergence, there is neither a total flux of matter into the system, nor out of it, as it should be, since mass conservation must hold at each order of the expansion separately.

The reduced electrophoretic mobility is then finally calculated as

$$\mu_{red} = \frac{|\mathbf{u}^{(1)}|}{|\mathbf{E}_{ext}|}, \quad (39)$$

where $\mathbf{u}^{(1)}$ is the constant velocity of the colloid in the system's center-of-mass reference frame, i. e. (assuming no-slip boundary conditions) the value of the flow velocity field at the surface of the colloidal sphere,

$$\mathbf{u}^{(1)} = \mathbf{v}^{(1)}(R), \quad (40)$$

with R the radius of the particle. This mobility is strictly independent of the strength of the external driving field.

3. Computational method

3.1. Iterative procedure

The linearisation of the problem divides the challenge of solving the electrokinetic equations into two different subproblems. For the zeroth order, a solution of the fully nonlinear Poisson–Boltzmann equation must be found. The first order consists of a set of linear equations, where the zeroth order fields only occur as prefactors. Here we need to solve the Poisson equation, the convection–diffusion equation and the incompressible Stokes equation. Each particular problem can then be dealt with by using a specialised solver, which is some finite-difference scheme on a regular lattice with periodic boundary conditions; details for each solver will be outlined below. Finally all methods are combined via iterative loops, as sketched in Fig. 1.

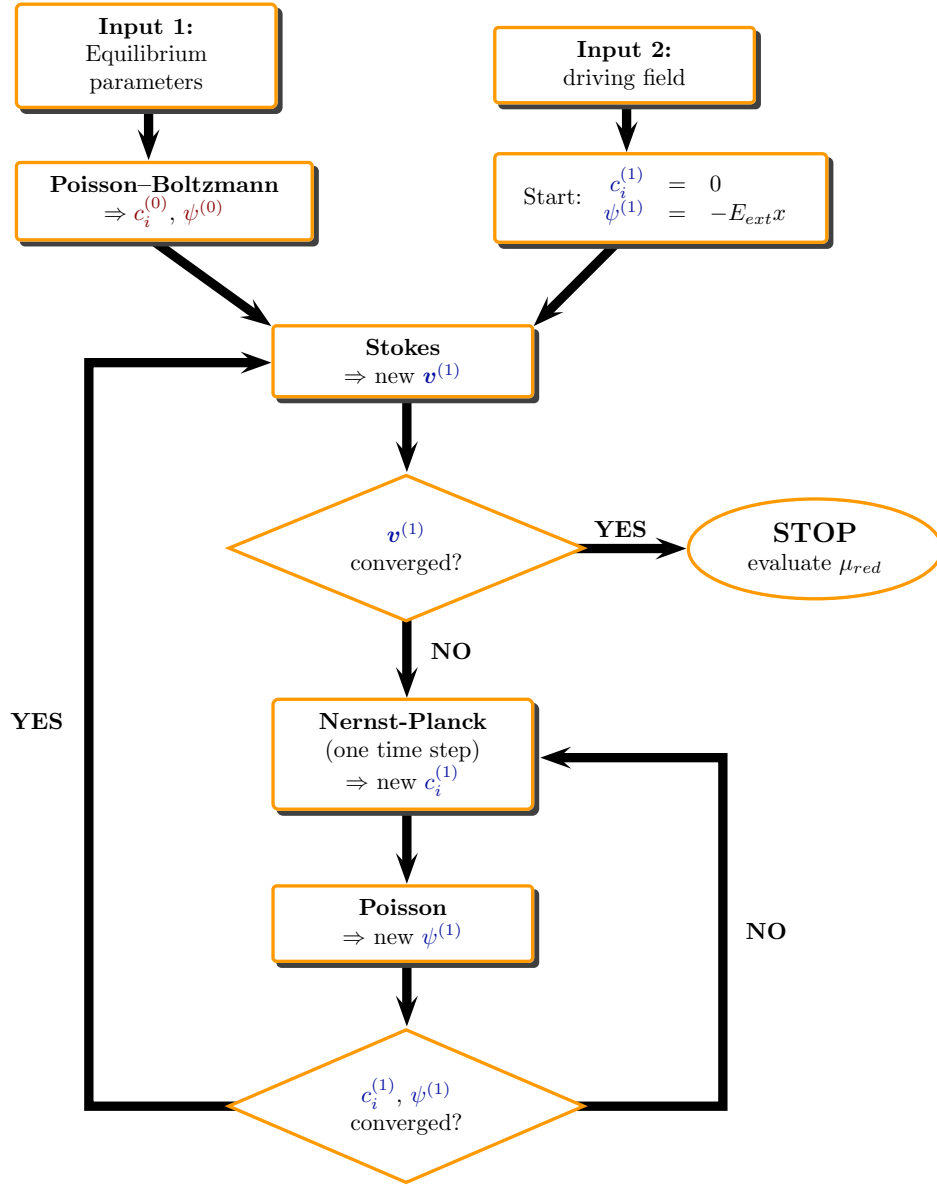


Figure 1. Schematic illustration of the iterative algorithm for solving the electrokinetic equations.

It turned out that the convergence of the method is improved by not using the full new velocity field for the next iteration, but rather a convex combination of the result of the previous iteration and the most recent result of the Stokes solver \mathbf{v}^* :

$$\mathbf{v}^{(1)} \leftarrow \omega \mathbf{v}^* + (1 - \omega) \mathbf{v}^{(1)}, \quad 0 < \omega \leq 1; \quad (41)$$

in practice we used $\omega = 1/2$. The iteration procedure yields a sequence of reduced mobilities $\mu_{red}^{(i)}$, $i = 1, 2, \dots$; the iteration was terminated as soon as the relative residual

$$\varepsilon = \left| \frac{\mu_{red}^{(i)} - \mu_{red}^{(i-1)}}{\mu_{red}^{(i)}} \right| \quad (42)$$

dropped below the value 10^{-5} .

3.2. Poisson-Boltzmann equation

For the zeroth order a solution of the fully nonlinear Poisson–Boltzmann equation is required. Here, a simple and unconditionally stable lattice algorithm has been used, based on a constrained variational approach of the Poisson–Boltzmann equation. This method has been discussed in detail in Ref. [29] and is hence only be briefly summarised here. It should be noted that this method has prompted other groups to develop similar ideas even further [25]; however, such more recent implementations have not been used here.

Following the ideas of Maggs and Rosetto [30] and re–formulating the equations in terms of the electric field instead of the electrostatic potential, Eqs. 24 and 25 are written as

$$\nabla \cdot \mathbf{E} = \sum_i z_i c_i, \quad (43)$$

$$\nabla \times \mathbf{E} = 0, \quad (44)$$

$$z_i \mathbf{E} = \nabla \ln c_i. \quad (45)$$

These equations are recovered as the Euler–Lagrange equations of a constrained free energy functional of the form

$$\mathcal{F} = \int_V f dV, \quad (46)$$

$$f = \frac{1}{2} \mathbf{E}^2 + \sum_i c_i \ln c_i - \psi (\nabla \cdot \mathbf{E} - \sum_i z_i c_i) - \sum_i \mu_i (c_i - \frac{N_i}{V}), \quad (47)$$

where the electrostatic potential ψ and the chemical potential μ_i of ionic species i occur as Lagrange multipliers taking into account Gauss’ law and mass conservation, respectively. N_i is the total number of ions of the species i and V denotes the system’s volume. Note that the formulation in terms of the electric field assures that the solution of the Poisson–Boltzmann equation is a true minimum of the functional. Applying a Yee discretisation [31], i. e. associating scalar fields with the sites, polar vectors with the links, and axial vectors with the plaquettes of a simple–cubic lattice, the functional can be minimised making local moves between adjacent nodes along a link and local field updates on the plaquettes. If the system has been initialised such that the constraints are fulfilled, those local moves never leave the constraint surface. Moreover, the update rules can be optimised, such that the functional value is decreased in every iterative step, and the method will run ultimately into the one and only minimum. For further details the reader is referred to Ref. [29].

3.3. Poisson equation

The Poisson equation for a given charge density can be solved efficiently by Fast Fourier Transform. We expand the potential and the charge density in terms of Fourier series

via

$$\psi(\mathbf{r}) = \sum_{\mathbf{k}} \hat{\psi}(\mathbf{k}) \exp[-i\mathbf{k} \cdot \mathbf{r}], \quad (48)$$

$$\rho(\mathbf{r}) = \sum_{\mathbf{k}} \hat{\rho}(\mathbf{k}) \exp[-i\mathbf{k} \cdot \mathbf{r}], \quad (49)$$

with

$$\mathbf{k} = 2\pi(k/L_x, l/L_y, m/L_z), \quad k, l, m \in \mathbb{Z}. \quad (50)$$

Here, $L_x \times L_y \times L_z$ is the dimension of the computational domain. The solution of the Poisson equation in Fourier space is then given by

$$\hat{\psi} = \frac{1}{\mathbf{k}^2} \hat{\rho}. \quad (51)$$

For consistency reasons we use a discretised version, i. e. a lattice Green's function, instead of the continuum Green's function [32]; the discretised counterpart to Eq. 51 reads

$$\hat{\psi}(k, l, m) = \frac{1}{\xi_{k,l,m}^2} \hat{\rho}(k, l, m) \quad (52)$$

with

$$\xi_{k,l,m}^2 = \frac{2}{a^2} \left\{ 3 - \cos\left(2\pi \frac{k}{N_x}\right) - \cos\left(2\pi \frac{l}{N_y}\right) - \cos\left(2\pi \frac{m}{N_z}\right) \right\}, \quad (53)$$

where a denotes the lattice spacing and $N_x = L_x/a$ etc. Back-transformation finally yields the desired electrostatic potential in real space.

3.4. Stokes equation

The stationary incompressible Stokes equation has the form

$$\nabla \cdot \mathbf{v}(\mathbf{r}) = 0, \quad (54)$$

$$-\nabla p(\mathbf{r}) + \eta \nabla^2 \mathbf{v}(\mathbf{r}) = -\mathbf{f}_{ext}(\mathbf{r}), \quad (55)$$

where \mathbf{f}_{ext} is an external force density and η denotes the fluid viscosity (which takes the value $2/3$ in our reduced unit system). For the purposes of the present paper, one should view \mathbf{f}_{ext} as the force density generated by the electric field and the charges. More precisely, we include in \mathbf{f}_{ext} all electric forces that come from the ion clouds, but also the force density that is generated from the fixed charges of the immersed body (or bodies). Since the total system is charge neutral, the total force on the system vanishes, even in the presence of external driving:

$$\int_V d^3r \mathbf{f}_{ext}(\mathbf{r}) = 0. \quad (56)$$

Again, it is obvious that this statement holds for the full nonlinear theory, and this implies that it must also hold separately at each order of the perturbation expansion. We now assume that the immersed bodies are not moving relatively to each other (cf. the remark at the end of Sec. 2.1), and also not rotating. Under these circumstances,

the flow field can be calculated rather straightforwardly, making use of the idea of replacing the differential equations by equivalent integral equations [33, 34]. This is done as follows: The boundary condition for the fluid is given by a unique constant (but unknown) velocity on the surface. To assure this boundary condition, one may introduce an artificial “reaction force density” \mathbf{f}_{reac} located on the surface (with units: force per area). This force density needs to be determined self-consistently such that the superposition of the flow fields generated by the external forces and these reaction forces satisfies the boundary condition. This is in spirit quite analogous to the electrostatic problem of a metallic surface, where the problem of finding a constant electrostatic potential at the surface is solved by determining an appropriate induced charge density. It is clear that this reaction force density cannot exert a net force onto the system, and hence we know

$$\int d\Omega \mathbf{f}_{reac}(\mathbf{r}) = 0; \quad (57)$$

here Ω denotes the surface.

We thus can write the total flow field \mathbf{v} as a superposition of \mathbf{v}_1 , the contribution from the external force density, and \mathbf{v}_2 coming from the reaction force density:

$$\mathbf{v}(\mathbf{r}) = \mathbf{v}_1(\mathbf{r}) + \mathbf{v}_2(\mathbf{r}) \quad (58)$$

$$\mathbf{v}_1(\mathbf{r}) = \int_V d^3r' \overset{\leftrightarrow}{\mathbf{T}}(\mathbf{r} - \mathbf{r}') \mathbf{f}_{ext}(\mathbf{r}'), \quad (59)$$

$$\mathbf{v}_2(\mathbf{r}) = \int d\Omega' \overset{\leftrightarrow}{\mathbf{T}}(\mathbf{r} - \mathbf{r}') \mathbf{f}_{reac}(\mathbf{r}'), \quad (60)$$

where $\overset{\leftrightarrow}{\mathbf{T}}$ is the Green’s function of the Stokes equation.

For an infinite fluid this Green’s function is well known and given by the Oseen tensor (see e. g. [35]). In Fourier space it is given by

$$\overset{\leftrightarrow}{\mathbf{T}} = \frac{1}{\eta \mathbf{k}^2} \left(\overset{\leftrightarrow}{\mathbf{I}} - \frac{\mathbf{k} \otimes \mathbf{k}}{\mathbf{k}^2} \right), \quad (61)$$

where \mathbf{I} denotes the unit tensor. In a finite box, the same form still applies; however, one needs to take into account that only wave vectors \mathbf{k} occur that are compatible with the box periodicity. Furthermore, $\mathbf{k} = 0$ must be excluded, since the problem is solved in the system’s center-of-mass reference frame. This yields for the real-space counterpart

$$\overset{\leftrightarrow}{\mathbf{T}}(\mathbf{r}) = \frac{1}{V\eta} \sum_{\mathbf{k} \neq 0} \frac{\exp[-i\mathbf{k} \cdot \mathbf{r}]}{\mathbf{k}^2} \left(\overset{\leftrightarrow}{\mathbf{I}} - \frac{\mathbf{k} \otimes \mathbf{k}}{\mathbf{k}^2} \right); \quad (62)$$

here V denotes the total volume of the box. It should be noted that we can thus consider \mathbf{v}_1 as known, while we do not know \mathbf{v}_2 and \mathbf{f}_{reac} .

Now, picking two points \mathbf{r}_Ω and \mathbf{r}_{ref} that are both located on the surface, we know that their velocity must be identical:

$$\mathbf{v}_1(\mathbf{r}_\Omega) + \mathbf{v}_2(\mathbf{r}_\Omega) = \mathbf{v}_1(\mathbf{r}_{ref}) + \mathbf{v}_2(\mathbf{r}_{ref}), \quad (63)$$

$$\mathbf{v}_2(\mathbf{r}_\Omega) - \mathbf{v}_2(\mathbf{r}_{ref}) = \mathbf{v}_1(\mathbf{r}_{ref}) - \mathbf{v}_1(\mathbf{r}_\Omega), \quad (64)$$

$$\begin{aligned} & \int d\Omega' \left(\overleftrightarrow{\mathbf{T}}(\mathbf{r}_\Omega - \mathbf{r}_{\Omega'}) - \overleftrightarrow{\mathbf{T}}(\mathbf{r}_{ref} - \mathbf{r}_{\Omega'}) \right) \mathbf{f}_{react}(\mathbf{r}_{\Omega'}) \\ &= \mathbf{v}_1(\mathbf{r}_{ref}) - \mathbf{v}_1(\mathbf{r}_\Omega). \end{aligned} \quad (65)$$

In a discretised version the Ω' integral is replaced by a sum. If we now view \mathbf{r}_{ref} as an arbitrary but fixed reference point, while we vary \mathbf{r}_Ω , we may view Eq. 65 as a system of linear equations to determine \mathbf{f}_{react} . If the number of surface points is M , then the number of equations is $3M$, while the number of unknowns is $3M$ as well. However, three of these equations are redundant, since at the point $\mathbf{r}_\Omega = \mathbf{r}_{ref}$ only the trivial information $0 = 0$ is obtained. Instead, we need to use Eq. 57 as last set of equations to obtain a unique solution. In practice, the set of equations was solved numerically using the standard BiCGStab procedure [36, 37].

For discretisation, we again use a simple-cubic lattice with spacing a . For consistency reasons, we need to use the discrete version of the Oseen tensor, analogously to the lattice Green's function of the Poisson equation (see Eqs. 52 and 53 and Ref. [32]). The discretised Oseen tensor is derived by applying a midstep finite-difference scheme in real space, and doing the corresponding discrete Fourier transform with integer indexes k, l, m :

$$\hat{\overleftrightarrow{\mathbf{T}}}(k, l, m) = \frac{1}{\eta \xi_{k,l,m}^2} \left(\overleftrightarrow{\mathbf{I}} - \frac{\mathbf{q}_{k,l,m} \otimes \mathbf{q}_{k,l,m}}{q_{k,l,m}^2} \right) \quad (66)$$

with

$$\mathbf{q}_{k,l,m} = \frac{1}{a} \left\{ \sin\left(2\pi \frac{k}{N_x}\right), \sin\left(2\pi \frac{l}{N_y}\right), \sin\left(2\pi \frac{m}{N_z}\right) \right\}, \quad (67)$$

$$\xi_{k,l,m}^2 = \frac{2}{a^2} \left\{ 3 - \cos\left(2\pi \frac{k}{N_x}\right) - \cos\left(2\pi \frac{l}{N_y}\right) - \cos\left(2\pi \frac{m}{N_z}\right) \right\}. \quad (68)$$

3.5. Convection-diffusion equation

Equation 35 is the stationary limit of a convection-diffusion equation of the general form

$$\left(\frac{\partial}{\partial t} + \nabla \cdot \mathbf{w}(\mathbf{r}) \right) c(\mathbf{r}, t) = D \nabla^2 c(\mathbf{r}, t) + S(\mathbf{r}, t). \quad (69)$$

Here $c(\mathbf{r}, t)$ denotes the ionic concentration field of first order at the spatial position \mathbf{r} and time t . The convective term is not the fluid velocity, but rather the coupling term of the first order ion concentration with the zeroth order electrostatic potential, $\mathbf{w}(\mathbf{r}) = -Dz \nabla \psi^{(0)}(\mathbf{r})$. The source term $S(\mathbf{r}, t)$ contains all other terms independent of the first-order ion concentration field. Equation 35 is a conservation law, and therefore

$$\int d^3r c(\mathbf{r}, t) = \text{const.}, \quad (70)$$

$$\int d^3r S(\mathbf{r}, t) = 0. \quad (71)$$

The latter equation states that no ionic particles are produced or annihilated during the process. The discrete counterpart of such an equation is a Master equation, the

coefficients of which need to be adjusted such that its continuum limit recovers Eq. 69. A detailed and systematic derivation of such an algorithm shall be published separately [38]. In the present work, we use the simplest version, which is a nearest-neighbour model on the simple-cubic lattice, which has lowest-order accuracy, and present the algorithm without proof. The concentration fields are initialised as zero at every lattice site and then propagated using a Master equation of the form

$$c(\mathbf{r}, t) = \sum_i A_i(\mathbf{r} - a\mathbf{\Delta}_i) c(\mathbf{r} - a\mathbf{\Delta}_i, t - h) + hS(\mathbf{r}, t - h), \quad (72)$$

where h is the discretisation time step, \mathbf{r} denotes the lattice sites and a is the lattice spacing. $\mathbf{\Delta}_i$ denotes a dimensionless lattice vector connecting \mathbf{r} with one of its neighbours, such that $\mathbf{r} + a\mathbf{\Delta}_i$ is again a lattice site. For our simple three-dimensional nearest-neighbour model, $i = 1, \dots, 6$, and the transfer coefficients are given by

$$A_i(\mathbf{r}) = \frac{1}{6} \left(1 + \frac{a}{2D} \mathbf{w}(\mathbf{r}) \cdot \mathbf{\Delta}_i \right), \quad (73)$$

while the diffusion constant is

$$D = \frac{1}{6} \frac{a^2}{h}. \quad (74)$$

This means that the continuum limit is obtained by Taylor expansion up to second order with respect to only one variable a , since the time step is not a variable that can be picked independently from a , but rather is given by $h = a^2/(6D)$.

4. Numerical results

4.1. Parameters

From now on, we will return to the notation of Sec. 2.2 and, for reasons of clarity, distinguish between dimensional and reduced quantities.

The electrophoretic mobility μ_{red} is a dimensionless quantity, and hence it can only depend on dimensionless parameters as well. In Ref. [23] we discussed, within the framework of the present Mean-Field treatment, a finite system with added salt, where all ion types have the same properties, i. e. all ions are monovalent and have all the same friction coefficient. We then found as one possible set of dimensionless parameters:

(i) the reduced charge

$$\hat{Z} = Z \frac{l_B}{R} = \frac{\tilde{Z}}{4\pi\tilde{R}}, \quad (75)$$

(ii) the rescaled colloid radius $\tilde{R} = \kappa R$, (iii) the rescaled diffusion constant of the ions \tilde{D} (as defined in Tab. 1) and (iv) a dimensionless quantity f_0 that specifies the fraction of counterions (species zero) relative to the salt ions. In general f_i is the fraction of the ionic species i relative to all ions in the system,

$$f_i = \frac{N_i}{\sum_j z_j^2 N_j}, \quad (76)$$

and it is easily shown that f_i is nothing but the volume-averaged concentration of ionic species i , in the reduced unit system of Tab. 1. For a system with only one salt species that has only monovalent ions, we know $f_1 = f_2$ (these fractions refer to the salt ions), and the sum rule $\sum_i z_i^2 f_i = 1$ implies that only one non-trivial parameter f_0 is left.

As already mentioned in Sec. 2.2, a definition of κ that is fully consistent with the finite-volume version of linearized Poisson-Boltzmann theory requires that the volume V is defined as the volume available to the ions. For a box of dimension $L \times L \times L$ and N colloidal spheres of radius R this means

$$V = L^3 - \frac{4\pi}{3}NR^3. \quad (77)$$

In our notation, N is the number of colloids and Z is their charge, while N_0 and z_0 are the number and valence of counterions, respectively, such that charge neutrality implies

$$NZ = -N_0z_0. \quad (78)$$

The colloid volume fraction is thus given by

$$\Phi = \frac{\frac{4\pi}{3}NR^3}{V + \frac{4\pi}{3}NR^3} \quad (79)$$

or

$$\frac{4\pi}{3} \frac{NR^3}{V} = \frac{\Phi}{1 - \Phi}. \quad (80)$$

Therefore the correct relation between volume fraction Φ and f_0 differs from the expression in Ref. [23] by a small correction term. Inserting Eqs. 19, 75, 76 and 78, one finds after a few lines of algebra

$$\frac{\Phi}{1 - \Phi} = -\frac{z_0 f_0}{3\hat{Z}}(\kappa R)^2 = -\frac{z_0 f_0}{3\tilde{Z}}\tilde{R}^2. \quad (81)$$

Furthermore, a dimensionless resolution d is defined such that for given d a sphere is always discretised by the same number of lattice sites:

$$d = \frac{\tilde{a}}{\tilde{R}}, \quad (82)$$

where \tilde{a} denotes the lattice spacing in reduced units and \tilde{R} is the radius of the particle, also in reduced units.

4.2. Comparison with previous results

Figure 2 studies the reduced mobility for a system consisting of one colloidal sphere in a box, where the volume fraction $\Phi \simeq 7.07 \cdot 10^{-3}$ as well as the reduced charge $\hat{Z} = 8, 10$ are kept fixed. The counterions are monovalent. \tilde{R} is varied by changing f_0 (cf. Eq. 81), i. e., by varying the salt content (one species, all salt ions monovalent). The calculations were done with a reduced diffusion constant $\tilde{D}_i = 1.5$ for all ionic species, and the resolution was kept fixed at the value $d = 0.07$. One clearly sees that the mobility systematically decreases with \tilde{R} , which is easily explained by the corresponding increase of electrostatic screening. Note that the present representation is given for constant \hat{Z} , which differs

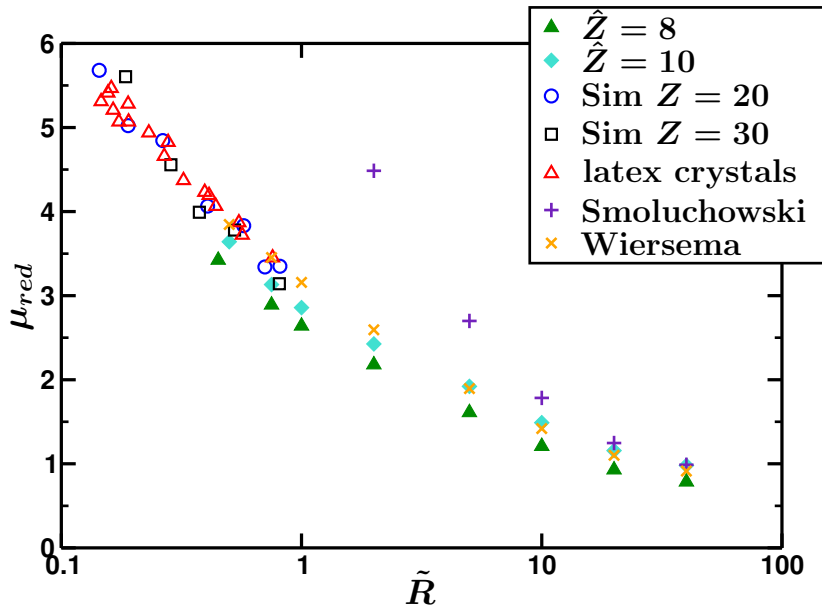


Figure 2. Reduced mobility as a function of \tilde{R} . The open symbols are results from Ref. [22].

from the classical calculations [9, 10, 11, 12, 13] that keep the zeta potential fixed, i. e. the electrostatic potential at the colloidal surface.

Furthermore, Fig. 2 shows also data from Ref. [22] (open symbols). The circles and squares are simulation results obtained from the Molecular Dynamics / lattice Boltzmann (MD/LB) raspberry model [39]. In the simulations a single colloid of charge $Z = 20$ ($Z = 30$) and radius $R_C = 3$ ($R_C = 5$) is surrounded by counterions. Both systems were studied with a Bjerrum length of $l_B = 1.3$, resulting in a reduced charge of $\hat{Z} = 8.5$, comparable to our value. The triangles are experimental results for latex crystals in a bcc structure with a particle size of $R = 34nm$ in a deionised aqueous suspension. The effective charge is quoted as $Z \simeq 450$ determined from conductivity measurements [40], resulting in a reduced charge of order $\hat{Z} \simeq 10$. In all cases of Ref. [22] the colloidal size and charge were fixed and salt ions were absent (except for the self-dissociation of water). The screening parameter, or \tilde{R} , was hence changed by varying Φ , while f_0 was kept constant (cf. again Eq. 81). This is qualitatively different from our numerical calculations, where rather Φ is kept constant and f_0 is varied. Nevertheless, the results seem to agree quite nicely, and within the accuracy of the data it seems that it does not matter whether the screening is salt-dominated or counterion-dominated. In the following subsection, we will put this question under more detailed and more accurate scrutiny.

Besides the question of the screening mechanism, there are also additional differences between our calculation and Ref. [22], in view of which the observed small discrepancies are hardly surprising: The MD/LB simulations use a slightly different reduced charge, and also the reduced diffusion constant of the ions is probably somewhat

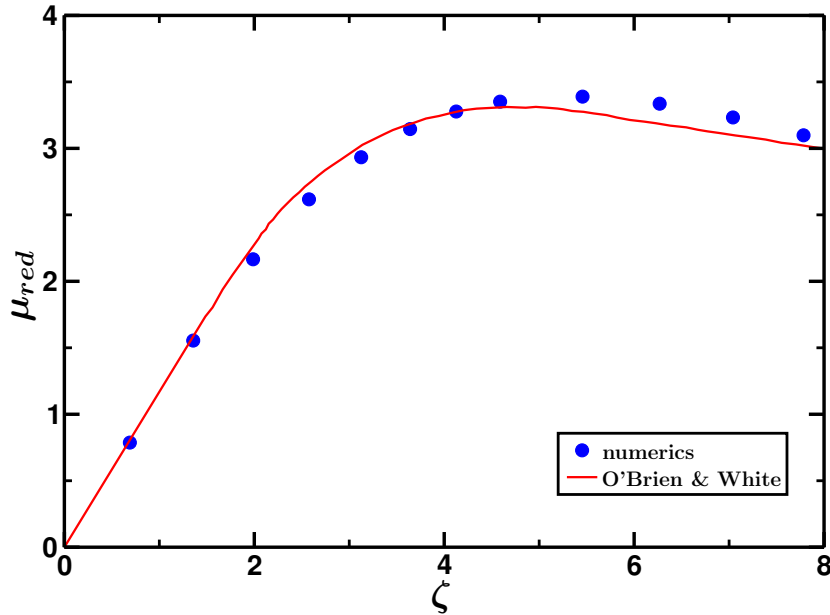


Figure 3. Reduced mobility as a function of the dimensionless (reduced) zeta potential (determined from the solution of the Poisson–Boltzmann equation) for $\tilde{R} = 8$, $d = 0.07$, $\tilde{D} = 1$ and $f_0 \simeq 0.01$. The solid line is the result taken from Ref. [13].

different. The influence of the diffusion constants on μ has so far not been thoroughly studied; in the next subsection it will be shown that μ increases with the D_i , as one might expect. For the experiments, the situation is even less clear, since there is a considerable amount of ambiguity in the mapping of the effective charge of the real physical system to the bare charge in the Mean-Field calculations.

Finally, Fig. 2 presents also a comparison with two theoretical results. Firstly, the Smoluchowski limit [6] of the reduced mobility is given by

$$\mu_{red}^{Smo} = \frac{3}{2}\zeta_{red}, \quad (83)$$

where ζ_{red} is the reduced (dimensionless, cf. Tab. 1) zeta potential, i. e. the electrostatic potential at the colloid surface. This can be easily calculated within our approach; it is just a result of our Poisson–Boltzmann solver, where we take for ζ the potential difference between colloid surface and box boundary. Secondly, within an approximate numerical theory for a single colloid in an infinite salt solution, Wiersema et al. [11] have tabulated values for μ_{red} as a function of ζ_{red} and \tilde{R} , while the influence of \tilde{D}_i is stated there to be fairly small. We can therefore use our values for \tilde{R} and ζ_{red} to also compare with that theory, using linear interpolation. While the Smoluchowski limit is reached for values $\tilde{R} \simeq 40$, the data obtained from the work of Wiersema et al. describe our numerical results quite well over the full range.

Since our method is the extension of O’Brien and White’s work [13] to systems with finite volume fraction and a finite amount of counterions, it should produce identical results in the limit of strongly salt-dominated screening ($f_0 \rightarrow 0$), where the ionic

cloud of the colloid does not overlap with those of its periodic images. A quantitative comparison is however hampered by the fact that Ref. [13] does not tabulate its results, but only provides plots, and, more importantly, that the values of the ionic diffusion constants are not quoted. It seems however that $\tilde{D} = 1$ for all ionic species is reasonable; at least we do find quite good agreement between our calculations and Ref. [13] for this value, as demonstrated in Fig. 3.

4.3. Salt vs. counterion screening

The parameter f_0 can be used to quantify the screening mechanism. Values close to unity (for a monovalent system) indicate a system where the amount of counterions in the system is dominant, while a value close to zero means that the salt ions dominate the screening mechanism. In order to focus on the screening *mechanism* (salt screening vs. counterion screening), one should keep κ (or κR) strictly constant, while varying *only* f_0 . Within our numerical approach, this is easily possible: The computer experiment consists of adding more and more salt (in terms of concentration), which enhances the screening, while at the same time the box size is increased, such that the counterions are more and more diluted and their contribution to the screening is reduced. This is done in such a way that the total amount of screening remains constant (see Eq. 81). Of course, the reduced charge and the reduced diffusion coefficients are kept constant as well.

A common assumption is that only the screening length, but not the screening mechanism should contribute to the value of the electrophoretic mobility. Although Fig. 2 and previous studies [22] show that within the given accuracy the effect of f_0 on the mobility is at least weak, there is no fundamental reason why the mobility should be strictly independent of f_0 .

In order to test this quantitatively, we have studied (i) a single colloidal sphere in a box, corresponding to a simple-cubic (sc) crystal, (ii) two spheres in the box, such that the resulting crystal is body-centered cubic (bcc), and (iii) four spheres arranged in such a way to construct a face-centered cubic (fcc) crystal. The fixed parameters were $\tilde{R} = 1$, $\hat{Z} = 10$, $\tilde{D} = 1.5$, $d = 0.08$, while f_0 was varied. Since we work at constant resolution, the resulting curves (μ_{red} vs. f_0) in Fig. 4 are smooth. Indeed, the plot nicely shows that the reduced mobility does depend on the screening mechanism in a non-trivial fashion, for all three types of lattice structures. However, the effect is only of the order of 5 to 10%, and hence was not observable previously.

In order to assess the effect of the lattice resolution on this result, we analysed the sc case in some more detail by varying d as well. Due to computational limitations, this was however confined to a fairly narrow interval $0.06 \leq d \leq 0.09$. Nevertheless, a reasonably reliable linear extrapolation to the continuum limit $d \rightarrow 0$ seems possible, see Fig. 5, where this is shown for the data point $f_0 = 0.5$. The result of this extrapolation, namely the reduced mobility as a function of f_0 in the limit $d \rightarrow 0$, is presented in Fig. 6, where cubic splines were used for interpolation. Even though the data may not

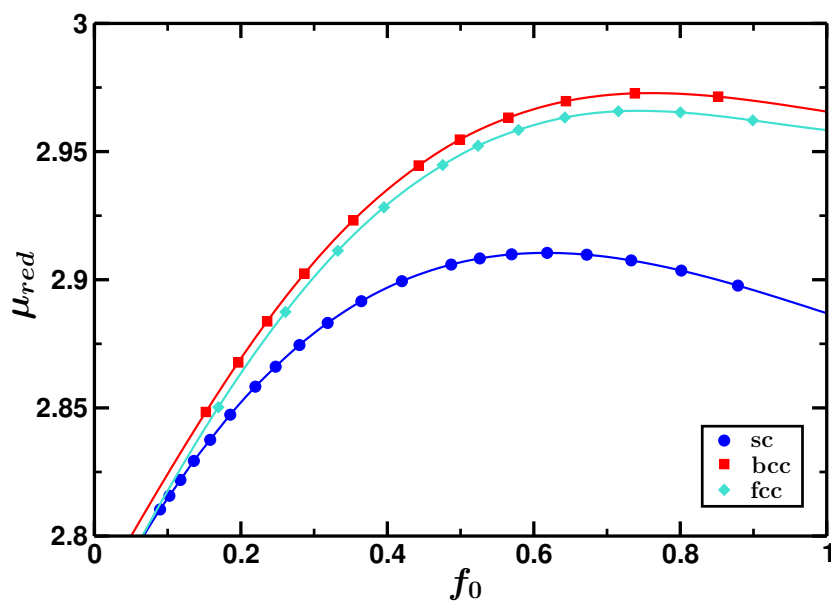


Figure 4. Reduced mobility as a function of f_0 for constant $\tilde{R} = 1$ and three types of lattice structure as indicated by the legend. Every sphere carries a reduced charge of $\hat{Z} = 10$ and the computational resolution is $d = 0.08$.

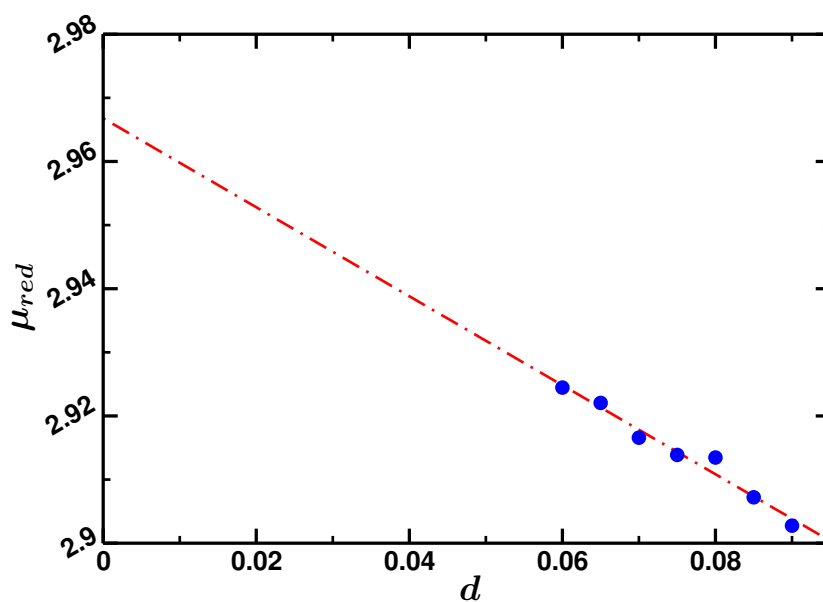


Figure 5. Reduced electrophoretic mobility as a function of the sphere resolution d for a constant value of $f_0 = 0.5$. The red line shows a linear fit to the numerical data.

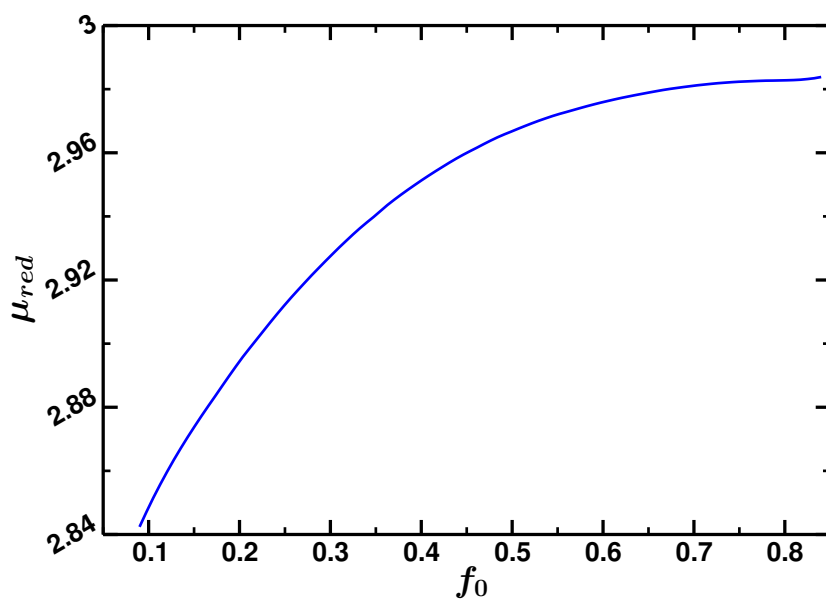


Figure 6. Reduced electrophoretic mobility as a function of f_0 in the continuum limit $d \rightarrow 0$.

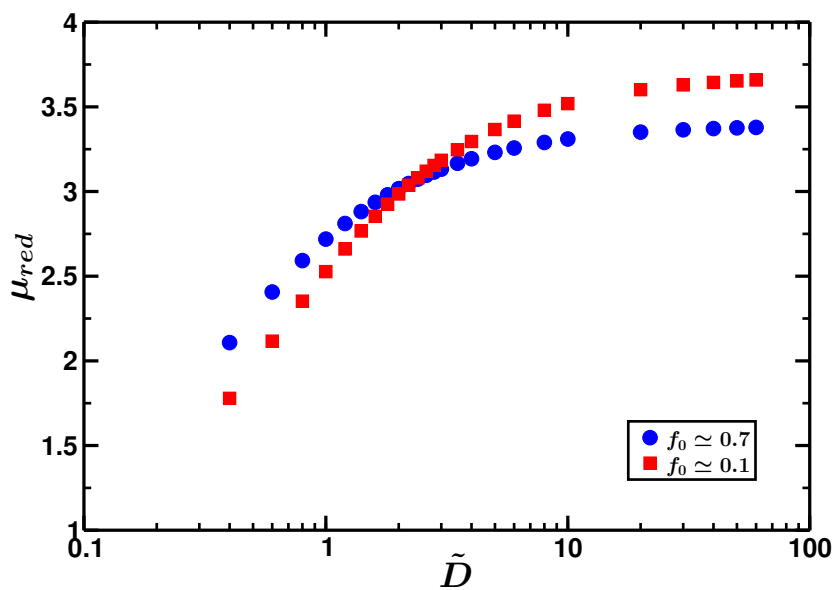


Figure 7. Reduced electrophoretic mobility as a function of the diffusion constant. Both curves are generated for a system with $\tilde{R} = 1$, $\tilde{Z} = 10$, $d = 0.07$ and various values of f_0 as indicated by the legend.

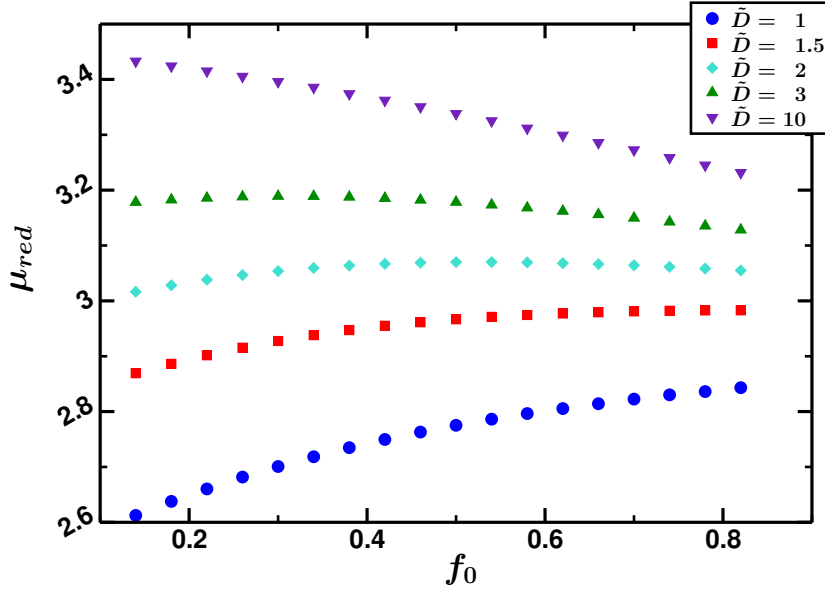


Figure 8. Reduced mobility as a function of f_0 for one single sphere in a periodic box (sc lattice) and the same parameters as in Fig. 4 for different diffusion constants as indicated by the legend. This plot shows $d \rightarrow 0$ extrapolated values.

be fully reliable due to the smallness of the d interval, they nevertheless indicate fairly convincingly that the effect is more than just a discretisation artifact.

Furthermore, it turns out that this non-trivial behaviour is even more interesting when studying the effect of the diffusion constants. The limiting behaviour for $D_i \rightarrow 0$ and for $D_i \rightarrow \infty$ can be easily understood. For $D_i \rightarrow 0$, only the convective part of the convection–diffusion equation remains:

$$\mathbf{v}^{(1)} \cdot \nabla c_i^{(0)} = 0. \quad (84)$$

At least for a single sphere in infinite space it is easily shown that this enforces the trivial solution $\mathbf{v}^{(1)} = 0$ (and hence $\mu = 0$): In a spherical coordinate system with origin at the center of the sphere, and polar angle relative to the driving field, it is clear that the radial component of $\mathbf{v}^{(1)}$ must vanish, due to the above condition, while the azimuthal component must be zero as well, due to symmetry. Therefore only the polar component remains. However, imposing the condition $\nabla \cdot \mathbf{v}^{(1)} = 0$ for that component yields a solution that is either singular (and hence forbidden) or zero. We hence find $\mu \rightarrow 0$ for $D_i \rightarrow 0$, and it is highly plausible that this holds in the general case as well. Conversely, the limit $D_i \rightarrow \infty$ means that the convective term can be ignored, and the problem becomes independent of D_i . Hence the electrophoretic mobility saturates at some limiting value.

These predictions are nicely confirmed in our calculations, see Fig. 7. The data shown there were calculated for $\tilde{R} = 1$, $\tilde{Z} = 10$ and $d = 0.07$, but for different screening mechanisms. Since the curves intersect, one sees that switching from salt-dominated to counterion-dominated screening may either enhance the mobility (this happens for

small diffusion coefficients) or reduce it (this is the behaviour at large D). In more detail, this behaviour is analysed in Fig. 8.

4.4. Weakly charged colloids

A very interesting phenomenon can be observed in the case of weakly charged colloids. Consider an uncharged spherical obstacle in a solution of negatively and positively charged ions. Applying a constant external electric field, electro-osmotic flow is generated by electric forces acting on the salt ions; positive charges move with the field direction, negative charged ions against it. Since the ions can not penetrate the solid sphere, the ion fluxes will be deflected by the particle. Thus, negative salt ions accumulate at one side of the sphere, while positive ions are depleted in that region. Since no electric forces act on the uncharged particle, the accumulation of positive ions at one side and negative ions at the opposite side must be symmetric. This accumulation effect leads to a polarisation of the system. Note that the induced dipole moment points in the “wrong” direction, i. e. anti-parallel to the driving field. This is interesting, because it is in contrast to the usual observation that for a charged sphere the induced dipole moment points in the “right” direction, i. e. parallel to the external field [21].

For an uncharged sphere in an infinite salt solution, the problem is dramatically simplified and amenable to an exact analytical solution; this was recently presented by Dhont and Kang [41]. In reduced units their result for the dipole moment is

$$\tilde{\mathbf{p}} = -2\pi\tilde{R}^3\tilde{\mathbf{E}}_{ext}. \quad (85)$$

Our numerical calculations nicely reproduce this prediction for a system with $\hat{Z} = 0$, $\tilde{R} = 1$, $\tilde{E} = 1$. However, again we need to reach the limit of an infinite system, meaning $\Phi \rightarrow 0$, as well as the continuum limit $d \rightarrow 0$. This double extrapolation is presented in Figs. 9 and 10, and our final numerical result is

$$\tilde{p} \simeq -6.23, \quad (86)$$

which deviates less than 1% from the expected value -2π .

In a second step, the reduced charge \hat{Z} of the colloidal sphere was increased, while we kept $\tilde{R} = 1$, $\tilde{E} = 1$ and used $\tilde{D} = 1.5$. The results for the dipole moment are presented in Fig. 11, and they will be discussed below.

We would like to comment that we believe that at this point the advantages of our perturbative approach come to full effect. In a non-perturbative calculation, the induced dipole moment would be a very weak signal on top of the leading-order charge cloud, and this weak contribution may be fairly difficult to be disentangled from artifacts in the leading order (discretisation errors and roundoff errors which result in an artificial nonzero dipole moment). Conversely, in our calculation the leading-order and the first-order contribution are cleanly separated. We hence believe our method to be more accurate and stable than non-perturbative approaches.

Returning to Fig. 11, we observe that the dipole moment increases with increasing charge. For a reduced charge of about $\hat{Z} = 2$, depending on the volume fraction, the

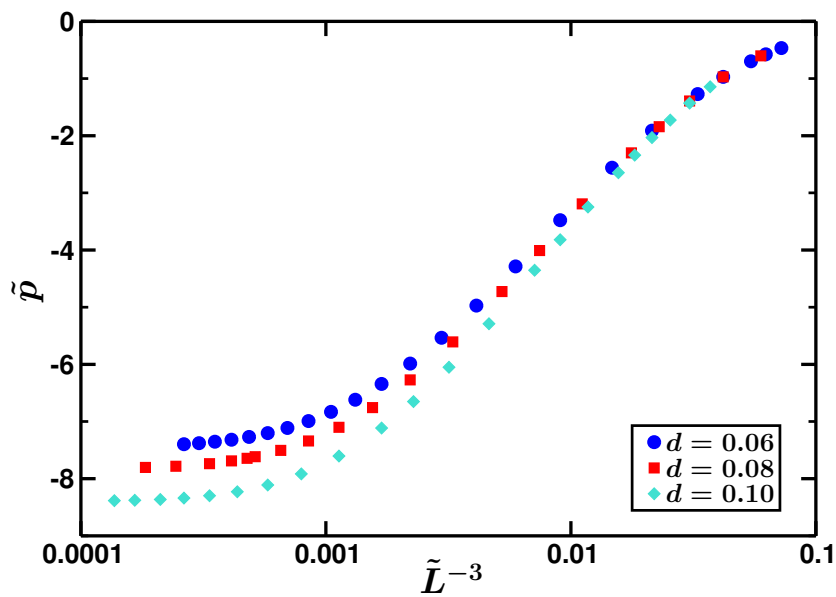


Figure 9. First order dipole moment as a function of the inverse box size for various resolutions as indicated by the legend.

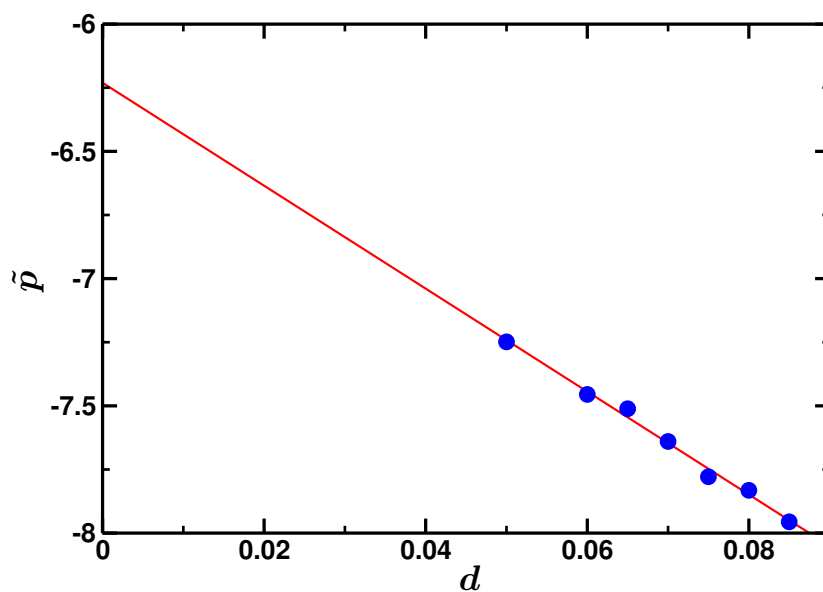


Figure 10. Dipole moment as a function of the resolution d , where the data points are the results of extrapolations to the $L \rightarrow \infty$ limit.

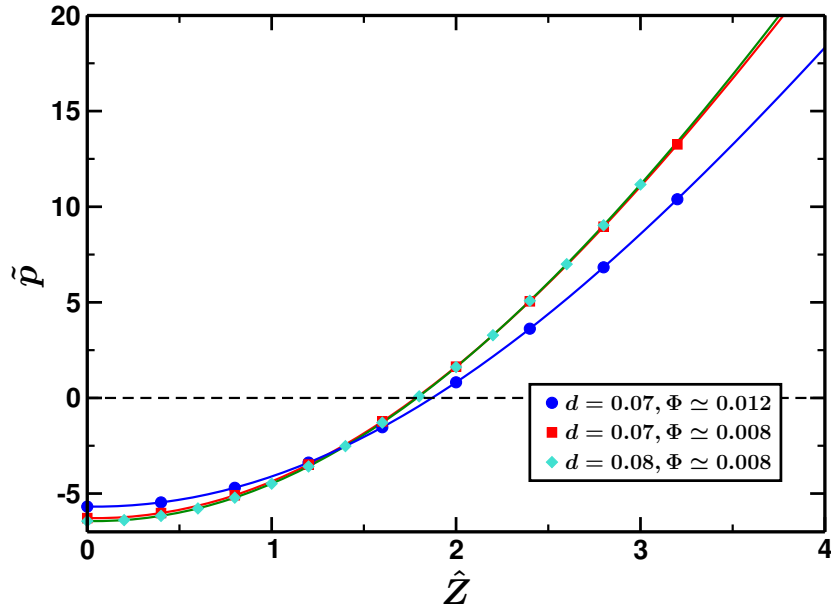


Figure 11. Dipole moment as a function of the reduced particle charge, for $\tilde{R} = 1$, $\tilde{E} = 1$, and various volume fractions and resolutions as indicated.

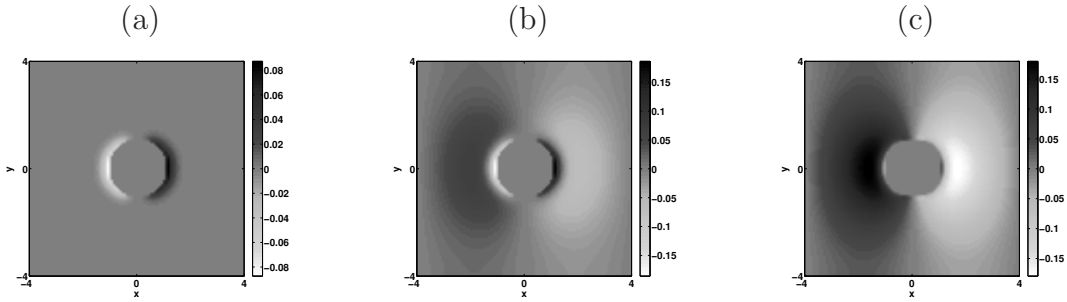


Figure 12. 2-dimensional cuts of the first-order concentration profile of the negative salt ions $\tilde{c}_-^{(1)}$, for the parameters $d = 0.08$, $\tilde{R} = 1$, $\Phi \approx 8.18 \cdot 10^{-3}$ and an electric field of $\tilde{E}_x = 1$ acting in the x direction. The reduced charges of the sphere and the dipole moments of the system are (a) $\hat{Z} = 0.0$, $\tilde{p}_x = -6.44$, (b) $\hat{Z} = 1.8$, $\tilde{p}_x = 0.087$ and (c) $\hat{Z} = 3.0$, $\tilde{p}_x = 11.16$.

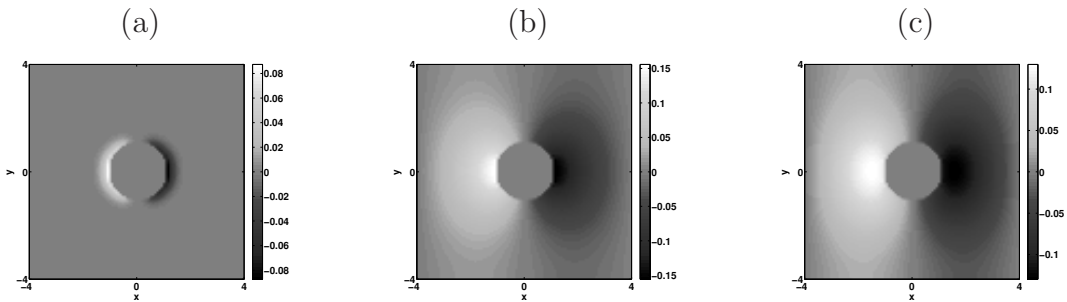


Figure 13. 2-dimensional cuts of the positively charged salt concentration $\tilde{c}_+^{(1)}$, for the same sets of parameters as in Fig. 12.

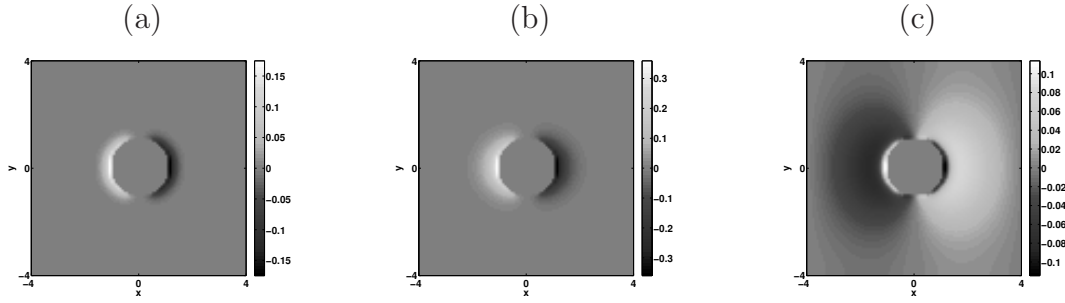


Figure 14. 2–dimensional cuts of the first order charge density $\tilde{\rho}^{(1)}$. The parameters are the same as in the previous images (see Fig. 12).

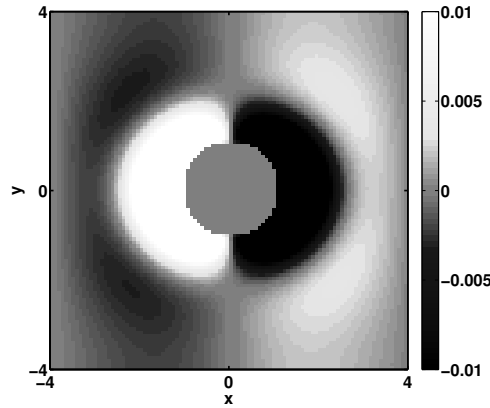


Figure 15. Same data as Fig. 14(b) but with rescaled colormap.

sign of the dipole moment changes, i. e. the orientation of the charge cloud is reversed. In order to elucidate the phenomenon in some more detail, we present in Figs. 12, 13 and 14 the first–order charge clouds as two–dimensional cuts in the xy plane (the field is oriented in x direction): Figure 12 depicts the negative salt ions, Fig. 13 the positive salt ions and Fig. 14 the charge density. Most interesting are the figures in the case of a very small but already “normal” dipole moment: Here one sees that the orientation of the charge cloud near the colloid is still “anomalous”, but this is more than compensated from “normal” contributions further away. For the charge distribution, this cut is plotted again in Fig. 15 with a rescaled colormap for better visibility. All in all, this charge cloud reversal highlights that in electrophoresis both electrostatic and hydrodynamic effects are important, and that these may compete, resulting in a change of qualitative behaviour depending on conditions.

The critical charge, i. e. the value of the colloid charge at which the dipole moment switches its sign, depends on the volume fraction. Keeping all other parameters fixed as before and the resolution at $d = 0.07$, we mapped out the functions \tilde{p} vs. \hat{Z} and determined the critical value via spline interpolation. The dependence of this value on

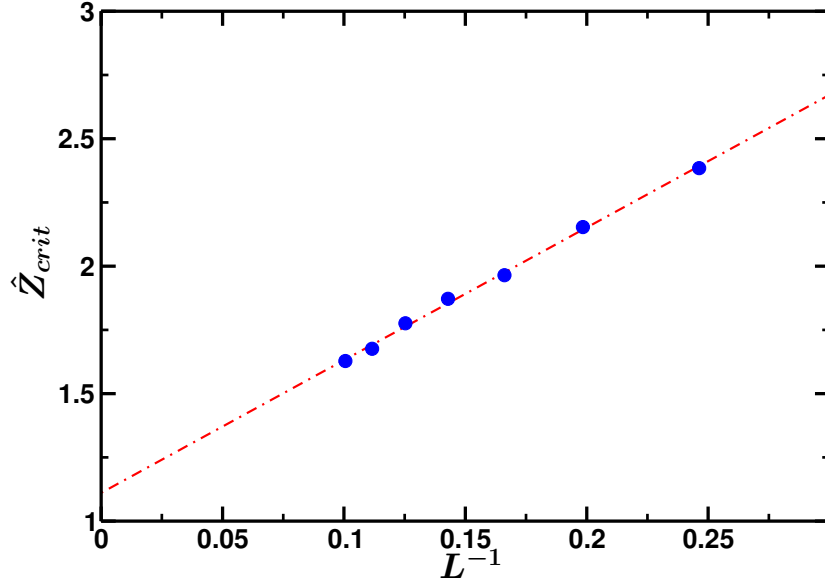


Figure 16. Critical charge as function of the inverse box length L^{-1} as obtained from the roots of spline functions. The line is a linear fit to the data points.

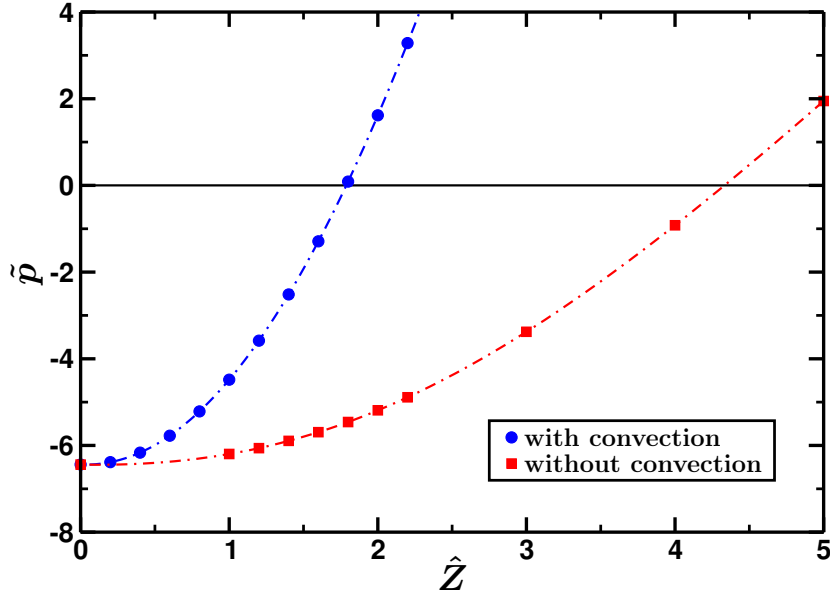


Figure 17. Dipole moment as function of the reduced charge for the same parameters as in Fig. 11. Here, we choose $d = 0.08$ and $\Phi \simeq 8.18 \cdot 10^{-3}$. The blue circles are the same data as before. For the red squares the convection velocity was set to $\tilde{v}^{(1)} \equiv 0$. The dash-dotted lines are cubic splines.

the linear system size L is shown in Fig. 16; extrapolation yields

$$\hat{Z}_{crit}(\Phi \rightarrow 0) = 1.11 \pm 0.02. \quad (87)$$

Finally, Fig. 17 demonstrates that the charge cloud reversal is fairly strongly affected by the value of the ion diffusion coefficient. To this end, we also studied the

case $D_i \rightarrow \infty$, which we realized computationally by just repeating our calculation with $\tilde{D} = 1.5$ but turning the convection term in the convection–diffusion equation off. Alternatively, one may therefore view this calculation as a study that elucidates the influence of convection. The result is clearly that convective transport helps in establishing the “normal” orientation.

5. Concluding remarks

In this paper we investigated a new numerical approach for the theoretical treatment of a charge–stabilised colloidal dispersion in an external electric field. The system, given by a solid charged sphere in an electrolyte solution, was treated on a Mean–Field level, resulting in a system of coupled nonlinear partial differential equations. Following the ideas of O’Brien and White [13], the nonlinearity is confined to the equilibrium Poisson–Boltzmann equation by application of a linearisation with respect to the external field. The iterative procedure in combination with the chosen specialised solvers turns out to be very efficient and only limited by the choice of the lattice spacing. While the demand on memory for the bulk methods increases linearly with the number of grid nodes, the surface integral solver for the Stokes equation requires a dense matrix connecting all surface nodes of the colloidal particles. Thus, the amount of memory needed for the storage of this matrix increases rapidly with the resolution of the sphere. Therefore this method is very efficient up to a certain value of the resolution; beyond that, alternative solutions must be developed. However, the iterative method has the advantage that it is designed as a modular solver and every module can be replaced via an alternative algorithm. One possible approach for going to higher resolutions is to replace the Stokes solver by a bulk method. For example, the time step of a lattice Boltzmann method could be adjusted such that it is identical with the time step of the convection–diffusion solver. Thus, the iterative method could be modified in a way that the Nernst–Planck and the Stokes equation are solved simultaneously. Furthermore, the lattice Boltzmann method would have the same degree of locality as the convection–diffusion equation solver, and hence parallelisation using a domain decomposition would be easily implemented. Nevertheless, the current single–processor implementation is quite efficient and reliable for a fairly satisfactory range of parameters. The numerical results agree reasonably well with various established results from the literature.

Furthermore, all parameters in the method are controlled independently, which offered, e. g., the opportunity to study the dependence of the electrophoretic mobility on the diffusion coefficient of the surrounding ions. One of the most interesting results presented above is the conclusion that the screening mechanism has an effect on the electrophoretic mobility, i. e. the mobility varies by a few percent if the amount of salt is increased in the solution, while the screening length is kept constant. This shows clearly that the assumption that counterion–dominated systems may be mapped onto salt–dominated systems is only approximately true: If the accuracy goes beyond, say, 5%, special care must be taken for the exact screening mechanism. Moreover, this

dependence is also affected qualitatively by the diffusion coefficient.

Another very interesting application is the examination of weakly charged colloidal systems. If an electric field acts on an uncharged colloidal sphere in salt solution, ions move and are deflected at the surface of the solid particle, resulting in an “anomalous” dipole moment anti-parallel to the driving field. This “anomalous” dipole moment was recently addressed by Dhont and Kang [41] analytically. With our numerical method we were able to reproduce their result up to one percent difference. Increasing the colloid charge, we find a critical value at which the dipole moment changes its sign and the ion cloud reverses its orientation.

All in all, the developed tool is computationally much cheaper than the raspberry MD/LB model [39], while having a somewhat broader range of applicability than the original work of O’Brien and White [13]. Clearly, it has limitations, as outlined in more detail in the Introduction. Although it will therefore not be able to study all electrokinetic phenomena in charge-stabilised colloidal dispersions — in particular, many-colloid systems where the particles continuously move with respect to one another, and a global rest frame does not exist, are out of reach for the present single-colloid version — we believe that it has already proven useful and is fairly likely to continue to do so.

Acknowledgments

This work was funded by the SFB TR 6 of the Deutsche Forschungsgemeinschaft. We thank J. K. G. Dhont, B. Li and A. J. C. Ladd for helpful discussions.

References

- [1] M. Evers, N. Garbow, D. Hessinger, and T. Palberg. Electrophoretic mobility of interacting colloidal spheres. *Phys. Rev. E*, 57(6):6774–6784, 1998.
- [2] M. Medebach and T. Palberg. Phenomenology of colloidal crystal electrophoresis. *J. Chem. Phys.*, 119(6):3360–3370, 2003.
- [3] M. Medebach and T. Palberg. Electrophoretic mobility of electrostatically interacting colloidal spheres. *J. Phys. Condens. Matter*, 16:5653–5658, 2004.
- [4] N. Garbow, M. Evers, T. Palberg, and T. Okubo. On the electrophoretic mobility of isolated colloidal spheres. *J. Phys. Condens. Matter*, 16:3835–3842, 2004.
- [5] T. Palberg, M. Medebach, N. Garbow, M. Evers, A. B. Fontecha, H. Reiber, and E. Bartsch. Electrophoresis of model colloidal spheres in low salt aqueous suspension. *J. Phys. Condens. Matter*, 16:S4039–S4050, 2004.
- [6] M. von Smoluchowski. Contribution to the theory of electro-osmosis and related phenomena. *Bull. Intern. Acad. Sci. Cracovie*, pages 184–199, 1903.
- [7] E. Hückel. The cataphoresis of the sphere. *Phys. Z.*, 25:204–210, 1924.
- [8] D. C. Henry. The cataphoresis of suspended particles. Part I. The equation of cataphoresis. *Proc. R. Soc. A*, 133(821):106–129, 1931.
- [9] J. T. G. Overbeek. *Kolloidchem. Beihefte*, 54:287, 1943.
- [10] F. Booth. The cataphoresis of spherical, solid non-conducting particles in a symmetrical electrolyte. *Proc. R. Soc. A*, 203:514–533, 1950.

- [11] P. H. Wiersema, A. L. Loeb, and J. T. G. Overbeek. Calculation of electrophoretic mobility of a spherical colloid particle. *J. Colloid Interface Sci.*, 22:78, 1966.
- [12] H. Ohshima, T. W. Healy, and L. R. White. Approximate analytic expressions for the electrophoretic mobility of spherical colloidal particles and the conductivity of their dilute suspensions. *J. Chem. Soc., Faraday Trans. 2*, 79:1613–1628, 1983.
- [13] R. W. O’Brien and L. R. White. Electrophoretic mobility of a spherical colloidal particle. *J. Chem. Soc., Faraday Trans. 2*, 74:1607–1626, 1978.
- [14] C. S. Mangelsdorf and L. R. White. Electrophoretic mobility of a spherical colloidal particle in an oscillating electric field. *J. Chem. Soc., Faraday Trans.*, 88(24):3567–3581, 1992.
- [15] M. Lozada-Cassou, E. González-Tovar, and W. Olivares. Nonlinear effects in the electrophoresis of a spherical colloidal particle. *Phys. Rev. E*, 60:17–20, 1999.
- [16] M. Lozada-Cassou and E. González-Tovar. Primitive model electrophoresis. *J. Coll. Int. Sci.*, 239(2):285–295, 2001.
- [17] H. Ohshima. On the general expression for the electrophoretic mobility of a soft particle. *J. Colloid Interface Sci.*, 228:190–193, 2000.
- [18] N. A. Mishchuk and S. S. Dukhin. Electrophoresis of solid particles at large Peclet numbers. *Electrophoresis*, 23:2012–2022, 2002.
- [19] F. Capuani, I. Pagonabarraga, and D. Frenkel. Discrete solution of the electrokinetic equations. *J. Chem. Phys.*, 121(16):973–986, 2004.
- [20] K. Kim, Y. Nakayama, and R. Yamamoto. Direct numerical simulations of electrophoresis of charged colloids. *Phys. Rev. Lett.*, 96:208302, 2006.
- [21] V. Lobaskin, B. Dünweg, and C. Holm. Electrophoretic mobility of a charged colloidal particle: A computer simulation study. *J. Phys. Cond. Matt.*, 16(38):S4063, 2004.
- [22] V. Lobaskin, B. Dünweg, M. Medebach, T. Palberg, and C. Holm. Electrophoresis of colloidal dispersions in the low-salt regime. *Phys. Rev. Lett.*, 98(17):176105, 2007.
- [23] B. Dünweg, V. Lobaskin, K. Seethalakshmy-Hariharan, and C. Holm. Colloidal electrophoresis: Scaling analysis, Green–Kubo relation, and numerical results. *J. Phys. Cond. Matt.*, 20:404214, 2008.
- [24] S. Allison, H. Wu, U. Twahir, and H. Pei. Conductivity and electrophoretic mobility of dilute ionic solutions. *J. Colloid Interface Sci.*, 352:1–10, 2010.
- [25] S. Zhou, Z. Wang, and B. Li. Mean-field description of ionic size effects with non-uniform ionic sizes: A numerical approach. *Phys. Rev. E*, 84:021901, 2011.
- [26] H. M. Manzanilla-Granados, F. Jiménez-Ángeles, and M. Lozada-Cassou. The zeta potential for a concentrated colloidal dispersion: The colloidal primitive model vs. the cell model. *Colloids and Surfaces A: Physicochem. Eng. Aspects*, 376(1):59–66, 2011.
- [27] H. M. Manzanilla-Granados, F. Jimenez-Angeles, and M. Lozada-Cassou. Polarity inversion of zeta-potential in concentrated colloidal dispersions. *J. Phys. Chem. B*, 115:12094–12097, 2011.
- [28] W. B. Russel, D. A. Saville, and W. R. Schowalter. *Colloidal Dispersions*. Cambridge University Press, Cambridge, 1989.
- [29] M. Baptista, R. Schmitz, and B. Dünweg. Simple and robust solver for the Poisson–Boltzmann equation. *Phys. Rev. E*, 80(1):016705, 2009.
- [30] A. C. Maggs and V. Rossetto. Local simulation algorithms for Coulomb interactions. *Phys. Rev. Lett.*, 88(19):196402, 2002.
- [31] K. Yee. Numerical solution of initial boundary value problems involving Maxwell’s equations in isotropic media. *IEEE Trans. Antennas and Propagation*, 14:302–307, 1966.
- [32] W. H. Press, S. A. Teukolsky, W. T. Vetterling, and B. P. Flannery. *Numerical Recipes in C*. Cambridge University Press, 2nd edition, Cambridge, 1992.
- [33] G. K. Youngren and A. Acrivos. Stokes flow past a particle of arbitrary shape: A numerical method of solution. *J. Fluid Mech.*, 69:377–403, 1972.
- [34] A. A. Zick and G. M. Homsy. Stokes flow through periodic arrays of spheres. *J. Fluid Mech.*, 115:13–26, 1982.

- [35] L. D. Landau and E. M. Lifschitz. *Fluid Mechanics*. Butterworth-Heinemann, Oxford, 2000.
- [36] J. Dongarra, A. Lumsdaine, R. Pozo, and K. Remington. IML++ v. 1.2 users' guide, <http://math.nist.gov/iml++/>.
- [37] A. Meister. *Numerik linearer Gleichungssysteme*. Friedr. Vieweg & Sohn, Braunschweig/Wiesbaden, 1999.
- [38] R. Schmitz and B. Dünweg. In preparation.
- [39] V. Lobaskin and B. Dünweg. A new model for simulating colloidal dynamics. *New J. Phys.*, 6:54, 2004.
- [40] P. Wette, H. J. Schöpe, and T. Palberg. Comparison of colloidal effective charges from different experiments. *J. Chem. Phys.*, 116(24):10981–10988, 2002.
- [41] J. K. G. Dhont and K. Kang. Electric-field-induced polarization and interactions of uncharged colloids in salt solutions. *Eur. Phys. J. E*, 33:51–68, 2010.